



New tsunami runup relationships based on long wave experiments



Ingrid Charvet^{a,*}, Ian Eames^b, Tiziana Rossetto^a

^a Civil, Environmental and Geomatic Engineering, UCL, Gower Street, London WC1E 6BT, UK

^b Mechanical Engineering, UCL, Torrington Place, London WC1E 7JE, UK

ARTICLE INFO

Article history:

Received 10 September 2012

Received in revised form 21 May 2013

Accepted 24 May 2013

Available online 7 June 2013

Keywords:

Tsunami

Runup

Experimental modelling

Long waves

Regression analysis

ABSTRACT

Tsunami are propagating waves characterized by long wavelengths and large amplitudes close to the shore. They may also have a profile characterised by a large trough preceding the positive wave. These waves are destructive, causing severe damage to structures and human casualties when they reach coastal areas (e.g., Indian Ocean, 2004; Japan, 2011). Runup is a local characteristic of a wave flow inland and this measure, easily identifiable in the field, is extensively used as an indicator of tsunami inundation and impact on the coast.

In this paper, an innovative large scale experimental programme is applied to develop runup equations for long propagating waves. A pneumatic generator with a controlled valve system, capable of exchanging large volumes of water with the propagation flume is used. This novel generation system allows waves to be generated that have much larger wavelengths than those experimentally reproduced to date. Moreover, it enables leading depressed waves to be stably generated and analysed for the first time.

To analyse the influence of wavelength and wave shape on runup, the experimental data was partitioned into groups classified by wave period T/T_b (where T_b is the travel time of a linear wave along the length of the beach) and wave shape (elevated or N-waves). In this paper, elevated waves refer to waves of translation having a single positive elevation above mean water level, and N-waves refer to waves of translation comprising both a negative elevation (below mean water level) and a positive elevation. Dimensional analysis (using experimentally determined wavelength, potential energy and wave amplitudes) was applied to identify correlated measures. A statistical analysis was used to determine a power law relationship between runup and measures of the waveform, and to test the significance of the power law hypothesis. The experimental results show how both the wavelength and wave shape influence the runup distance. For $\frac{T}{T_b} < 1$, the runup is seen to scale as $R \sim a$, while for $\frac{T}{T_b} > 1$, it scales as $R \sim \sqrt{a}$.

© 2013 Elsevier Ltd. All rights reserved.

1. Introduction

Tsunami are commonly caused by undersea earthquakes that displace the seafloor, resulting in a disturbance at the ocean surface. The volume of water displaced now has potential energy to be transferred away from the source. Because the vertical seafloor displacement results in the deformation of the overlying water surface, large earthquakes (with moment magnitude $M_W > 7$) have the potential for generating tsunami.

Surface waves in the ocean are characterized by periods of seconds and wavelengths of about 10–100 m. Tidal movement is characterized by a time scale of 12 h and a wavelength set by the size of the local basin (e.g., 100 km). In comparison, the typical period and wavelength of a tsunami are intermediate, between ocean waves and tides (e.g., 2400 s). Moreover, the characteristics of tsunami

change significantly as they propagate across oceans, with amplitudes of a few centimetres offshore and wavelengths tending to be much longer than the water depth (e.g., 200 km). When they move into the coastal region, the wavelength decreases significantly (e.g., 20 km) and the wave height increases, sometimes reaching 10–15 m. The energy of a tsunami is conserved as they move towards the coast because the dissipation caused by drag on the ocean floor is negligible. In most inhabited coastal regions the slope of the land is small, and 15 m of height corresponds to a large distance inland (e.g., 1.5 km for 1:100). The potential for ingress into land and damage to infrastructure is significant. A variety of wave forms and wave trains have been observed in the past, with either leading elevated waves or leading depressed waves.

A measure of the potential for an incident wave to ingress inland is the runup height R (Fig. 1). Runup is defined as the maximum inundation point above sea level of a wave incident to a beach. It is extensively used, compared to other wave characteristics, as an indicator of a wave's potential coastal impact. Given the difficulty of incorporating complex bathymetry and coastal fea-

* Corresponding author. Tel.: +44 (0) 7984248695; fax: +44 (0) 2073800986.

E-mail addresses: i.charvet@ucl.ac.uk (I. Charvet), i.eames@ucl.ac.uk (I. Eames), t.rossetto@ucl.ac.uk (T. Rossetto).

Notation

E_P	total wave potential energy	f	friction coefficient
E_P^+	potential energy of the positive wave component	g	acceleration due to gravity
E_P^-	potential energy of the negative wave component	h	water depth in the constant depth region of the flume
E_K	total wave kinetic energy	l_b	horizontal length of the sloping beach
E^*	a characteristic energy	S_x^2	variance of parameter x for a sample
H	wave height (trough-to-peak)	S_{p_x}	pooled standard deviation for a combination of samples for the same variable x
K, k	regression coefficients	t_0	time when $\eta(t) = 0.01\eta_{\max}$ prior to occurrence of the wave peak
L	wavelength	$t_k, t_{\log K}$	value of the t statistic for $k, \log K$
L^*	a characteristic length parameter	$t_{(N,c/2)}$	critical value from t distribution for N degrees of freedom and a level of significance c
R	wave runup	$t_{\eta_{\max}}$	time of occurrence of the wave peak
R_l	horizontal runup or inundation length	x	chosen wave parameter or input variable (i.e., $x \equiv a, T, R$)
R^2	statistical coefficient of determination	y	response variable
$SE_k, SE_{\log K}$	standard errors associated with the prediction of $k, \log K$	z_i	standardized residuals
SSE	sum of squared residuals	α, γ	empirical factors relating characteristic wave parameters to runup
SST	total sum of squares	β	angle of the sloping beach
T	wave period	ε	error term (regression)
$T1$	time taken for the still water level ($\eta \approx 0$) to reach η_{\max} during generation of the positive wave component	η	water surface elevation with respect to still water level
$T2$	duration of the negative wave component	ρ	density of water (in experiments $\rho_0 1000 \text{kg/m}^3$)
T_b	travel time of a linear wave along the beach length	σ, σ^2 , respectively	estimated standard deviation, variance for the population for the parameter considered
X	a measure of horizontal distance		
a	positive wave amplitude		
a^-	negative wave amplitude		
$c_{p_{\text{exp}}}$	wave speed (measured experimentally)/ phase celerity		
e_i	residuals		

tures in numerical models, simplified runup expressions are used for example within the insurance and risk assessment community to estimate the coastal impact of tsunami.

A critical review of the runup relationships shows that several approaches have been used to develop runup equations. Some existing studies (e.g., Plafker, 1965) have tried to relate runup to the initial disturbance that creates a tsunami, such as the vertical

displacement of the sea floor. However, most past studies have correlated runup with the wave amplitude; the latter parameter being determined mainly through experiments or in a few cases from historical data. It appears obvious that there are other important wave characteristics that may have a bearing on runup. Furthermore, whilst most past experimental studies have adopted relatively long waves, characterised by wavelengths that are larger

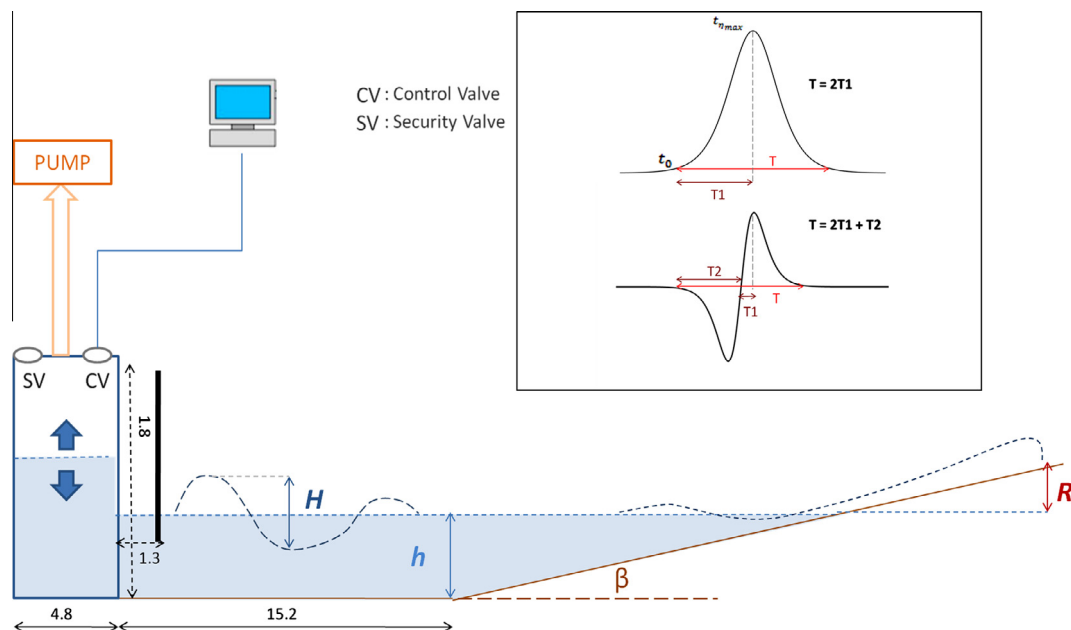


Fig. 1. Wave generator, general flume dimensions, wave probe and bathymetry. The numeric values are in meters. The runup height R is indicated, as the vertical distance above mean water level corresponding to the point of maximum wave inundation on the beach. The upper right corner schematic illustrates the method used to estimate the experimental wave period.

than the depth, these waves – mostly solitary waves – are not typically long as compared to the submerged beach. Moreover, while tsunamis have often been modelled experimentally using solitary waves, this theoretical wave shape may not always be representative of the geophysical wave (Madsen et al., 2008).

A critical review of the literature on runup equations also shows there to be a fundamental gap in understanding of the relationship between runup and the form of the incident waves. This is particularly true in the case of runup due to long depressed waves. The recent work of Klettner et al. (2012) analysed the draw down and runup of a depressed wave, and the results agreed generally with their analyses for relatively short waves, i.e., $L/h \sim 3$ (with L : wavelength and h : water depth). However, long depressed waves have been generally difficult to study because depressed waves generated by paddles are limited in wavelength by the stroke distance and are highly unstable (Kobayashi and Lawrence, 2004). The interaction between the incident and reflected wave in this typical experimental configuration sets an important constraint on the runup. There are currently no detailed studies of waves in this limit (i.e., long, depressed), and runup interactions for these cases. As a result, there is a significant gap in the current understanding of long-wave runup particularly in terms of the influence of wavelength, potential energy, mass etc.

How should the waves be characterized given this gap in our understanding? There are many metrics that could be applied to characterise the form and shape of an incident wave. It is useful to identify measures which do not change or change only by a small amount, as the wave evolves and moves towards a beach. The evolution of solitary wave amplitude is often described using the KdV equations. In this case there are an infinite number of invariants I_n defined in terms of the wave elevation η :

$$I_n = \int \eta^n dx, \quad (1)$$

where n is a positive integer. For inviscid fluids, Longuet-Higgins (1974) discusses a number of these invariants and specifically shows that I_1 and I_2 , which are related to the conservation of mass and potential energy, are conserved over water of constant depth. For a viscous fluid, I_2 is not conserved but changes slowly as the wave moves over a uniform channel due to the resistance caused by walls (Klettner and Eames, 2012). The benefit of characterising the wave shape in terms of I_1 is that quite strong statements can be made on how the wave ultimately evolves. For instance, for $I_1 > 0$, a train of solitary waves – a single solitary wave being a special case – will ultimately emerge along with a dispersive wave train, while for $I_1 < 0$, a solitary wave will not emerge. However, I_1 does not provide information about which component of the wave arrives at the beach first. Hence, a more phenomenological approach is usually applied to classify wave shape (e.g., elevated, leading depressed, N-wave etc). In the context of previous work, I_2 has been evaluated numerically but not experimentally (e.g., Klettner and Eames, 2012). In this study it is proposed to obtain experimental measures of I_2 .

The main purpose of this paper is to describe a new experimental study that analyses the correlation between runup and wave shape, characterised in terms of energy, amplitude, and wavelength. This experimental methodology is described in Section 3. This is followed by a comprehensive description of the statistical tools used to analyse the datasets and explore the dependence of runup on wavelength and shape. Within this study it is argued that the submerged beach length is a more appropriate parameter than water depth for the normalisation of the wavelength for wave classification – as also noted in the theoretical work from Madsen and Schaffer (2010), prior to the analysis and determination of runup regimes. Such a parameter provides an indication of the level of interaction of the wave with the beach. Indeed, processes such as

shoaling, reflections, and relative bottom friction will be affected by the relative length of the wave, therefore it is expected that the dynamics of runup will also be. The outcomes of the experimental runup study, in terms of empirical closures, are described in Section 4 along with a supporting physical explanation of the correlation groups. Conclusions are drawn in Section 5.

2. Overview of existing runup relationships

Early studies attempted to find a relationship between runup, wave height and wavelength for periodic waves incident on a beach (Kaplan, 1955; Shuto, 1967; Togashi, 1981), but no consistent trend developed, as highlighted by Synolakis (1986). The runup of propagating waves has been investigated analytically and numerically by using the momentum equations (Carrier and Greenspan, 1958; Kobayashi et al., 1990; Zelt, 1991), and also in the laboratory. The most widely used runup relationships found in the literature (Eqs. (2)–(6)), are listed in Table 1. These studies focus specifically on run up over impermeable beds and are discussed in greater detail below. In this paper, h refers to water depth, H refers to the wave height (trough-to-peak), and $\cot\beta$ refers to the slope of the beach (Fig. 1).

Most runup studies have considered a single positively elevated wave running-up a beach with a constant slope, and have looked at the influence of wave amplitude on runup. This is because many of these waves are weakly dispersive and do not significantly change shape as they propagate along a flume to the beach. The experimental waves generated in past studies tend to resemble solitary waves, are unidirectional, and propagate over a constant depth region. These include Hall and Watts (1953), who determine a general runup relationship of the form of (2), and Synolakis (1986). The latter complemented his experimental results with an analytical runup calculation using shallow water theory (3), which is valid for non-breaking waves. The runup was defined in the mathematical model as the maximum wave amplitude above the initial shoreline position, at the maximum penetration of the wave (also in Tadepalli and Synolakis (1996)). Runup regimes were observed to be different according to the breaking or non-breaking nature of the waves. Experimental results agree with (3) for non-breaking waves. However, the predicted trend moves away from the non-breaking wave data at higher amplitudes, suggesting that wave amplitude does not account for the total variability in runup for highly non-linear waves. Similarly to Eq. (2), Eq. (3) highlights a strong dependence of runup on wave amplitude and takes into account the beach slope.

Generally, previous research highlights that beach slope is an influential parameter on wave runup (i.e., Fuhrman and Madsen,

Table 1

Empirical wave runup relationships. R is the runup, h is the water depth, H is the total wave height, β is the slope angle, α and γ are functions of β , ϵ_g and p_0 are respectively a scaling and a steepness parameter, R_{so} is the runup of a Boussinesq solitary wave of the same height as the N-wave considered, Q is a function of L and γ_s (see Tadepalli and Synolakis, 1996), H_b is the height of bore collapse, C is a coefficient describing the efficiency of the conversion of potential energy to kinetic energy, and U_s is the speed of the bore at the shoreline (shoreline velocity). E_{pR} is the potential energy at the maximum runup point, $E_{pR} = 1 - \frac{E_R}{E_I}$, where E_I is the incident wave energy, E_B is the energy dissipated by breaking, and δ is an empirically determined parameter characterizing the shape of the runup tongue ($\delta \sim 0.18$).

Waveform	Dimensionless Runup (R/h)	Reference
Solitary	$\alpha(\frac{H}{h})^\gamma$	(2) Hall and Watts (1953)
Solitary	$2.831\sqrt{\cot\beta}(\frac{H}{h})^{5/4}$	(3) Synolakis (1987)
N-wave	$3.3\epsilon_g p_0^{1/4} Q(L, \gamma_s) \frac{R_{so}}{h}$	(4) Tadepalli and Synolakis (1996)
Bore	$\frac{U_s^2}{2gh} = \frac{CH_b}{2h}$	(5) Baldock and Holmes (1999)
Bore	$[\frac{E_{pR}}{1.5\delta}] (\frac{H}{h})$	(6) Li and Raichlen (2003)

Table 2
 Values of α and γ obtained by different studies on wave runup. (*) for non-breaking waves (for the empirical result, the coefficients have been determined with a line of best fit), (**) for breaking waves, when runup is measured at the maximum position of the advancing shoreline. (***) The authors provided α and γ obtained for the maximum value of R/h for different slopes. Methods: Empirical (E), analytical (A), numerical (N).

	Slope β	Range a/h	α	γ	Method
Hall and Watts (1953)	1	0.05–0.43	3.1	1.15	E
Synolakis (1987)*	19.85	0.005–0.048	12.6 (4.1)	1.25 (1.01)	A (E)
Synolakis (1987)**	19.85	0.056–0.633	1.11	0.58	E
Borthwick et al. (2006)***	5, 10,30,50	0.15–0.3; 0.0750.15; 0.012–0.03; 0.005–0.012	3.02	0.91	N
Present work	20	0.046–0.18	2.14	0.77	E

2008). The dependence of runup on this parameter appears complex. For example, the results from Li and Raichlen (2002) show that non-breaking waves runup higher for milder slopes, while breaking waves exhibit the opposite trend. In the field, shallow slopes bordering continental coasts are a common feature. The analysis of the 2011 Japan tsunami field-based data by Nassirpour (2012) indicates that local variations in slope along transects of the continental shelf (East coast of Japan) do not seem to correlate with high local variations in runup. Another interesting result from the numerical study of Borthwick et al. (2006) suggests that there is an upper value to the wave runup for beach slopes between 1:100 and 1:5 – irrespective of the wave height, which corresponds to Eq. (2) with $\alpha = 3.02$ and $\gamma = 0.91$. Table 2 summarizes the values for α and γ obtained in previous studies (Hall and Watts, 1953; Synolakis, 1987; Borthwick et al., 2006). Despite the range of slopes and variety of experiments, there are only weak variations in the empirical values of α and γ , with γ close to the value of 1 – result consistent with a contribution of H of the same magnitude as the runup itself. Without knowing the form of the functional relationships for α and γ , it is not possible to know from (2) how slope influences runup. Eq. (3) would indicate that the runup is larger on shallower beaches for non-breaking waves, which agrees with the results from Li and Raichlen (2002). Indeed, the effects of shoaling are paramount on shallower slopes. It is worth noting that the effects of bed friction on shallow slopes are also important, and may lead to some dissipation of wave energy.

The influence of wave shape on runup has been partially addressed in the analytical and numerical studies of Tadepalli and Synolakis (1994) and Tadepalli and Synolakis (1996), where waves with different profiles, namely solitary and N-waves, are treated separately. In particular, Tadepalli and Synolakis (1996) used a hybrid KdV-shallow water numerical model to propagate an N-wave and develop a general runup equation (4) applicable to different types of N-waves, numerically. The authors applied the methodology of Synolakis, 1987 to assess the influence of wave form on the analytical expressions for runup of different types of non-breaking N-waves. They found that the runup of a leading depressed N-wave is greater than the runup of an equivalent (i.e., same amplitude) leading elevation N-wave or solitary wave (runup law (3)). However, there are still significant and fundamental gaps in the understanding of the behaviour of trough-led waves, due to the difficulty in generating these waves experimentally, and the scarcity of available field observations.

Another wave type often assumed to represent tsunami is a bore, a common form of long wave, approaching the shoreline. The amplitude of long waves increases as they move into shallower waters until the point of wave breaking. With this approach the bore height is the main parameter to be related to runup. Baldock and Holmes (1999) analytically derived a runup equation for bores in their study of swash oscillations, by using laws of motion for a body with constant deceleration and the results of previous studies. These authors also took into account the type of energy transfer around the shoreline, and derived equation (5), which describes the unsaturated runup (i.e., runup corresponding to the first

swash) as a function of the flow velocity, or the bore height (H_b). The coefficient $C(\frac{1}{2} < C < 1)$ in (5) is a measure of the efficiency of converting kinetic to potential energy during runup.

A small number of studies provide additional information regarding other factors that may influence runup. Borthwick et al. (2006) showed numerically that for $a/h > 0.015$, the runup decreases as the friction coefficient increases, showing that bed friction can influence runup. For a frictionless case, Borthwick et al. (2006) found there was no change in runup regime at $a/h = 0.015$. In this case (3) would apply to all waves. Moreover, their results indicated for a given value of the friction coefficient, there is an upper limit to the runup irrespective of the beach slope. Synolakis (1986) suggested that breaking waves run up higher than non-breaking waves, and by generating bores of different lengths, highlighted a dependence between the displacement and duration of plate motion and the maximum runup, which would suggest that the wavelength influences runup. However, for bores with duration greater than 10.8 s, all runups tend to a common value, which Synolakis (1986) suggests is explained by the significant reflected wave generated at the beach. Finally, Li and Raichlen (2003) measured runup experimentally and applied an energy balance to obtain equation (6). The potential energy E_{p_r} at the time of maximum runup was estimated from a simple energy conservation model based on the total incident energy, E_i , and the energy dissipated during breaking, E_b . Values of $\frac{E_b}{E_i}$ are empirically determined using a numerical scheme. Their results indicate that runup is directly dependent on wave height, which is consistent with previous studies.

To conclude this section, a detailed review of current runup models shows that existing runup equations are based either on analytical and numerical studies, or on few sources of experiments, which mainly involved solitary waves and bores. Most runup equations are either empirical or based on energy dissipation but do not account for the wavelength or wave shape. There is common agreement that wave amplitude needs to be considered in the prediction of runup. The influence of beach slope has been taken into account in most runup equations, with steeper slopes predicting a higher runup for breaking waves, the opposite trend being observed for non-breaking waves. Runup as a function of the energy dissipated by the wave during breaking has been investigated; however, breaking processes are complex, and the dissipated energy varies with bed slope and wave profile. The influence of wavelength or wave packet length is rarely considered. While potential and kinetic energy are used as the basis of a number of approximate models, they are not assessed in the context of the wave form. Lastly, there are conflicting conclusions when runup is considered solely as a function of amplitude, especially when waveform is analysed. As Klettner et al. (2012) demonstrated, runup depends critically on the shape of the wave with leading elevated waves running up further than leading depressed. Therefore, it is important to know the contribution of wave shape to runup characteristics.

In the following analysis the parameters to be considered are $H, a, a^-, L, h, \beta, E_p, \rho$ and g . a corresponds to the positive amplitude

of any wave, a^- corresponds to the negative amplitude of an N-wave; and $|a| + |a^-| = H$ (for an elevated wave, $a = H$). E_p is the total potential energy of a given wave. For N-waves, this can be split into the potential energy of the trough, E_p^- , and the potential energy of the peak, E_p^+ (for elevated waves, $E_p^+ = E_p$). ρ is the water density, and g is the acceleration due to gravity.

3. Experimental methodology

3.1. Setup

The wave generator used in this study is described in Rossetto et al. (2011). The novel element of the generator is that it generates waves pneumatically by raising and lowering the water free-surface within an enclosed tank, placed at one end of the wave flume. This mechanism allows the generation of stable leading depressed waves. The tests were carried out at HR Wallingford, where the generator was placed at one end of a 45 m long and 1.2 m wide flume. At the other end of the flume a bathymetry was built with a sump next to the end wall. The sump prevented reflections from the highest waves reaching the end of the flume. Due to the dimensions of the wave generator the effective length along which the wave propagated was approximately 28 m (see Fig. 1).

A 1/20 sloping beach was constructed from concrete. This slope angle is consistent with previous studies where mild slopes have varied from 1/15 (Li and Raichlen, 2003), to 1/20 (Synolakis, 1987) to 1/24 (Klettner, 2010), to 1/35 (Grilli et al., 1994).

The water height was measured using 12 resistance probes distributed along the length of the flume and a probe monitor (manufactured in-house by HR Wallingford). The resistance probes were calibrated prior to each series of experiments due to their sensitivity to the conductivity of water. The sampling frequency was 50 Hz (so a temporal resolution of ± 0.02 s), and the accuracy of wave elevation measurements was ± 0.005 m. Runup was measured directly using a horizontal tape measure along the flume wall and recording the maximum penetration point of the first swash (accuracy ± 0.01 m), along the centre line of the channel i.e., mid-distance be-

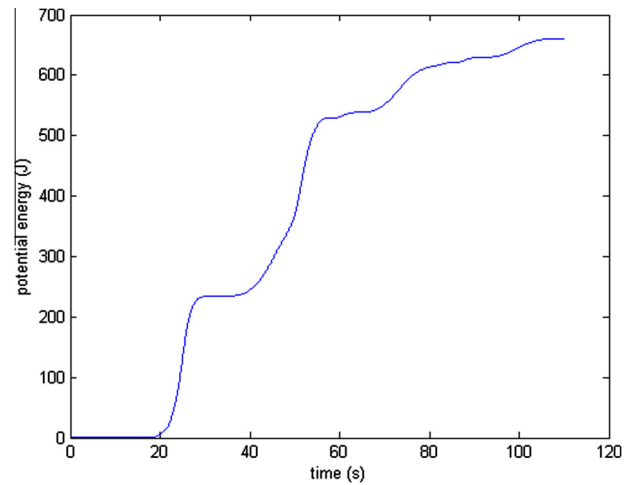


Fig. 3. Cumulative potential energy for the whole signal in a typical long elevated wave test. The first plateau reached corresponds to the input wave, the other plateaus to each other wave of the time series (reflections and sloshing).

tween the flume walls, in order to avoid edge effects. For the runup tests presented in this paper, the surface elevation nearest the wave generator was used to determine the wave parameters (see Fig. 1), and the ratios of a/h ranged between 0.02 and 0.18, for both elevated and N-waves.

The advantage of the adopted pneumatic generator is that long and leading depressed waves could be generated and were stable over the flume length. The wavelengths reproduced were much longer than the ones previously studied. The disadvantage was that some wave reflection occurred at the beach when elevated and leading elevated N-waves were created, due to the relative length of the waves.

3.2. Diagnostics

The measurement of runup is important for comparing the characteristics of the present waves with existing studies. Runup

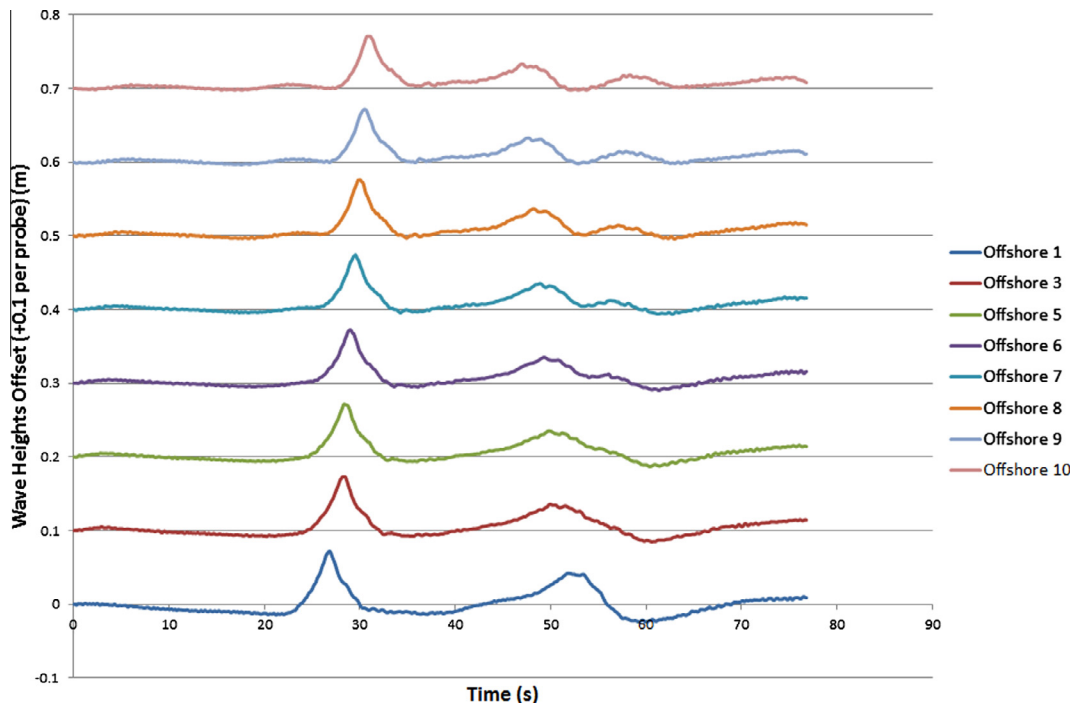


Fig. 2. Example of an experimental long elevated wave propagating along the length of the flume (constant depth region). Significant changes in the wave shape are not present, this result is typical of N-waves also (see Rossetto et al., 2011).

was estimated from the measured runup length R_l and converted to a vertical distance using:

$$R = R_l \tan \beta. \quad (7)$$

Wave period and wavelength were retrieved from the wave elevation time series. In many cases the second half of the positive part of the wave does not strictly correspond to the direct signal, due to the reflected waves travelling back from the beach. The period

Table 3

Pooled standard deviations (equation (A.2)) of positive and negative amplitudes, period, and runup, for elevated and N-waves. The first number in the brackets is the sample size (n) used to calculate the standard deviation for an individual sample s_x , the second number is the total number of waves $N(x)$.

Wave type	$S_{p_{ a }}$ (m)	S_{p_r} (s)	S_{p_R} (m)
Elevated waves	$2.1 \cdot 10^{-3}$ (4,9)	0.48 (4,9)	$3.4 \cdot 10^{-3}$ (6,25)
N-waves	$1.2 \cdot 10^{-4}$ (3,8)	$2.9 \cdot 10^{-2}$ (3,4)	$1.9 \cdot 10^{-3}$ (6,18)

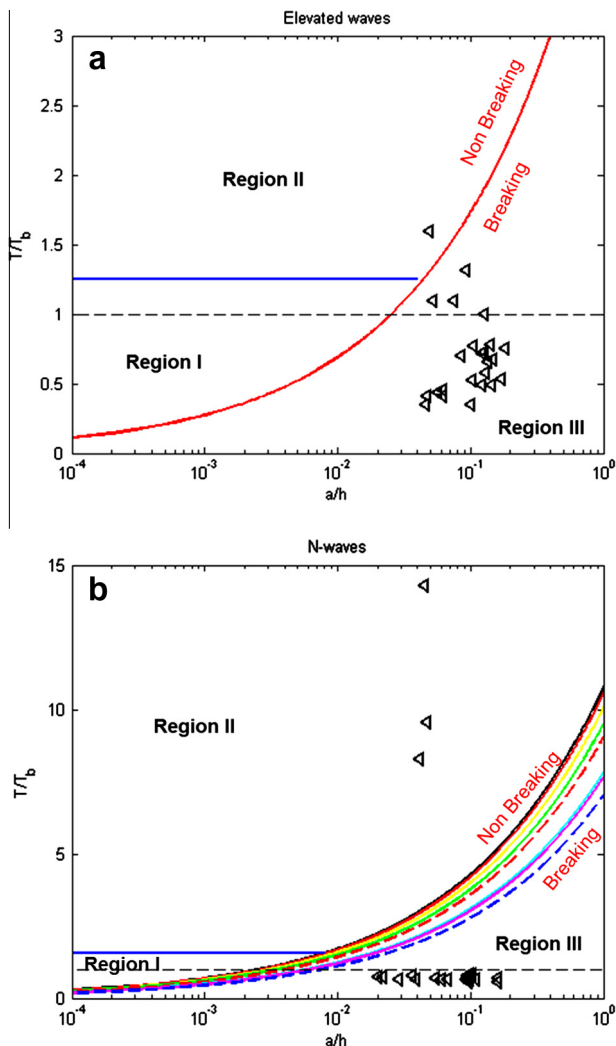


Fig. 4. Location of experimental elevated waves (a) and N-waves (b) within the regions defined using the non-linear shallow water theory following the methodology of Madsen and Schaffer, 2010. Region I corresponds to relatively short waves ($T/T_b < 5/4$ for single elevated waves, $T/T_b < 25/16$ for isosceles N-waves, these limits are shown in blue straight lines), Region II longer waves which are non-breaking, and Region III corresponds to the breaking region. Note: for N-waves (b), the breaking criterion depends on the trough-to-peak ratio, therefore the range of theoretical breaking criteria corresponding to the present N-waves have all been represented. (For interpretation of the references to colour in this figure caption, the reader is referred to the web version of this article.)

T and wavelength L are calculated using the first half of the positive wave, assuming symmetry (a schematic graph within Fig. 1 illustrates the method used to estimate the wave period):

$$T = 2(t_{\eta_{\max}} - t_0), \quad (8)$$

$$L = c_{p_{\text{exp}}} T. \quad (9)$$

In (8), $t_{\eta_{\max}}$ is the time of occurrence of the wave peak, and t_0 corresponds to the time when the value of the wave elevation is 1% of the maximum wave height ($t_{\eta_{\max}} > t_0$ and we set $T1 = t_{\eta_{\max}} - t_0$) prior to $t_{\eta_{\max}}$. In (9), $c_{p_{\text{exp}}}$ is the wave speed, determined from the experiments, by calculating the temporal correlation between adjacent wave probes. For N-waves, the trough does not trigger any reflections from the slope, so the parameters corresponding to the negative part of the wave are calculated on the full negative profile. The objective is to find a measure representative of the full wave shape, so integral measures of the wave as defined by Eq. (1) are used. Because excess mass can be positive, negative or equal to zero for N-waves, wave energy is the preferred integral parameter to be investigated, since it is always positive. The total potential energy E_p (per unit area width) wave is expressed at an instant time and is:

$$E_p = \int_0^{x_p} \frac{1}{2} g \rho_0 \eta(X)^2 dX. \quad (10)$$

To evaluate (10) requires knowledge of the wave profile in the entire flume at an instant in time. An estimate of (10) can be made by assuming that the wave slowly changes as it propagates over the length of the flume (this assumption has been checked by verifying wave elevation changes over the constant depth region – see Fig. 2 as an example). Approximately, $X = c_{p_{\text{exp}}} t$ so the potential energy of the wave in the constant depth region of the flume can be expressed as:

$$E_p = \int_0^{t_p} \frac{1}{2} g \rho_0 \eta(t)^2 c_{p_{\text{exp}}} dt, \quad (11)$$

where the integral is taken over a period of t_p . In these experiments, η is measured at generation, in the constant depth region of the flume (see probe position in Fig. 1). Due to sloshing and some reflections from the beach, multiple interacting waves are present in the whole time series. Predominantly, the initial wave for a given time series having a shorter period compared to the sloshing, the elevation data were truncated in order to remove the low frequency sloshing (see Charvet, 2012), and any potential reflection travelling in the opposite direction – indeed, all waveforms other than the initial wave can be dismissed without hindering the quality of the analysis. Moreover, the cumulative potential energy is calculated in order to identify the relative energy contribution of each wave packet. An example of the cumulative potential energy of a typical elevated wave time series is shown in (Fig. 3). The first energy plateau reached by the wave (at $t = t_p$) corresponds to the initial wave of the time series, the launched wave (the other plateaus correspond to subsequent waves), so the potential energy is calculated using the initial wave of the time series only.

The kinetic energy E_K of the wave was not evaluated. However, for long waves propagating without change of form over a uniform depth, it is easily demonstrated that $E_p = E_K$. As the wave propagates up the beach, there is an exchange between kinetic and potential energy. This is the basis of many of the models described previously for run up, such as Shen and Meyer (1963) and Li and Raichlen (2003). For this reason, the integral measure of the wave potential energy (10), (11) is used as an independent measure of the capability of the wave to move up the beach.

3.2.1. Repeatability

A critical element of the experimental study was to test the reproducibility of the measurements. The pooled standard deviation calculations are detailed in Appendix A, and the results discussed here are shown in Table 3. In comparison with the resolution of the spatial and temporal measurements (see Section 3.1), the standard deviation values indicate that the small variability is of the same order as the accuracy – with the exception of the period measurements for elevated waves where the variability is slightly higher – thus these small variations are an effect of the instrumental resolution only. In addition, taking $a_{\max,\min}$, $T_{\max,\min}$, and $R_{\max,\min}$ as the maximum and minimum amplitudes, periods and runups of the samples, respectively, the standard deviation of the measurements of these parameters were smaller than 7.4% of $|a_{\max,\min}|$, 8.4% of $|T_{\max,\min}|$ and 4.5% of $|R_{\max,\min}|$. The standard deviations of the samples s are representative estimates of total population standard deviation σ (i.e., standard deviation for all waves tested). Therefore, the experiments are repeatable.

3.2.2. Data split

A relative measure of the wave length should be defined to investigate runup. In the present experiments, variations in water depth (h) are small ($0.45 \text{ m} < h < 0.69 \text{ m}$), and it is believed that for long waves such as tsunamis the dynamics of wave runup will be mainly influenced by the length of the beach over which the wave travels, in comparison to the actual length of the wave. Because time series of wave elevation have been collected, we choose to consider the wave period as a representative measure of the wave length. The time T_b it takes for a given wave to travel the length of the beach l_b can be estimated:

$$T_b = \int_0^{l_b} \frac{dX}{\sqrt{gh(1 - \frac{X}{l_b})}} = \frac{2l_b}{\sqrt{gh}}. \quad (12)$$

Considering an average $h \approx 0.58 \text{ m}$ over the range of experiments, $l_b = 13.7 \text{ m}$, we obtain an approximate $T_b \approx 11 \text{ s}$. To distinguish between long and very long waves, we used the discriminator T/T_b as this provides a measure of the influence of beach length on the wave characteristics. For simplicity (and because the proportion of data would not change), we decided to use the critical value of $T/T_b = 1$ and split the data between long waves ($T/T_b < 1$) and very long waves ($T/T_b > 1$). The present experimental cases (T/T_b vs. a/h) have been placed in Fig. 4.

4. Experimental results

As a first step, the consistency of the new results with previous published studies is assessed. Next, the data is analysed through dimensional analysis taking into account the unique wave characteristics (i.e., in terms of shape, energy, wavelength). Finally, by applying a rigorous regression analysis, empirical runup relationships are derived and their associated uncertainty estimated. For the reader's convenience, the data (wave parameters as calculated using the aforementioned methods) have been listed in Appendix F.

4.1. Comparison with previous runup relationships

As previous experimental studies of runup largely looked at relatively short solitary waves, the consistency of the present experiments with known runup results can only be assessed using a representative subset of the present data (i.e., elevated waves for which $T/T_b < 1$). A regression analysis was applied to this subset, and it is found that the general runup equation from Hall and Watts (1953) (2) is consistent with long elevated wave runup for a slope of 1:20, when $\alpha = 2.14$ and $\gamma = 0.77$. Fig. 5 shows a compar-

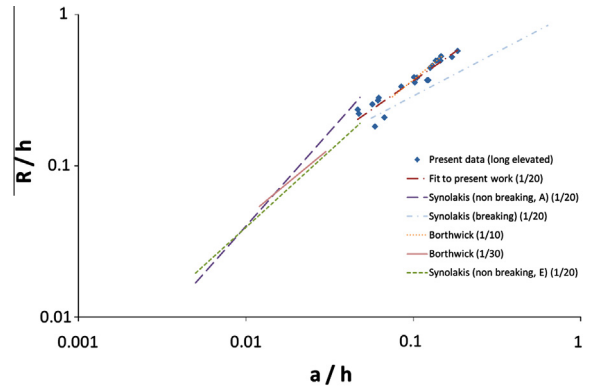


Fig. 5. Runup data for long elevated waves (present experiments), and relationships of the form of (2) obtained in previous studies for different values of α and γ as listed in Table 2.

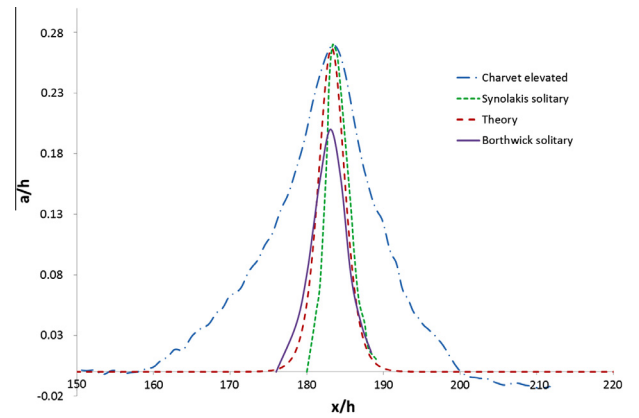


Fig. 6. Comparisons of wave profiles between typical elevated/ solitary wave for the runup studies considered in Fig. 3 (i.e., The present study, Synolakis, 1987; Borthwick et al., 2006 – numerical results and theory (Boussinesq first order solitary wave)).

ison between the long elevated wave data, the results of Synolakis (1987) and Borthwick et al. (2006) for beach slopes $10 < \cot \beta < 30$. Example wave profiles for the aforementioned studies are shown in Fig. 6. The waves in the present study are not as steep as classic solitary waves, but can be compared to these in terms of total height or area.

Moreover, it should be noted that the experimental waves generated were in the breaking region (both elevated waves and N-waves), for which analytical runup relationships do not exist. This has been illustrated in Fig. 4 also, which compares the present data with the analytical results from Madsen and Schaffer (2010).

The results presented in Table 2 show that the values of γ are relatively clustered ($0.582 < \gamma < 1.25$) for the empirically determined coefficients. This suggests that a linear relationship between wave height and runup may exist.

The present experimental waves follow the same trend as Synolakis' for a range of a/h ratios, but the new elevated waves – which overall wavelength and shape differ from typical (steeper) solitary waves generated in previous hydraulic models – have a higher runup (see Rossetto et al., 2011). Because Synolakis (1986) and Synolakis (1987) used a smooth aluminium beach, we would expect his waves to run up higher than the present waves, which were climbing a concrete slope with relatively greater roughness. However, the contrary is observed, which suggests wave amplitude is not the only parameter of importance, and that other measures such as wave length and/ or energy are paramount in determining wave runup.

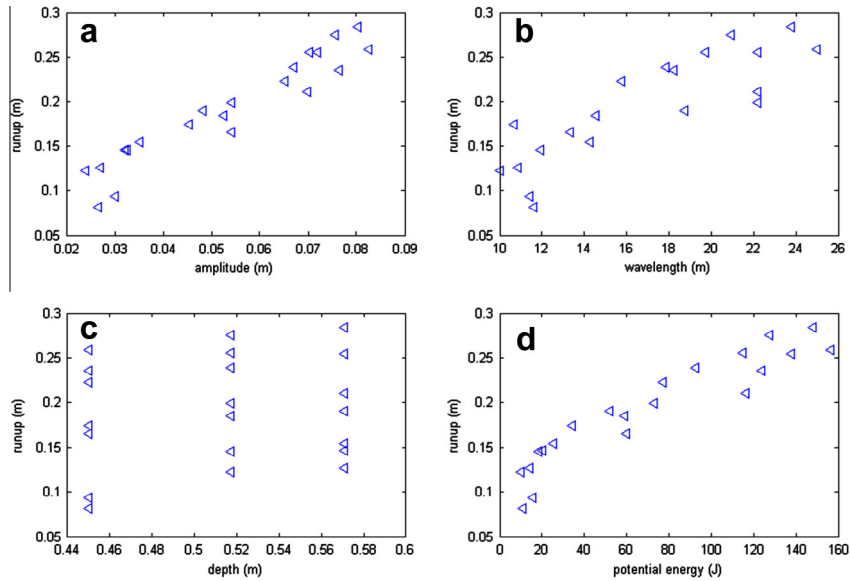


Fig. 7. Scatter plot of variables potentially influential on runup, here for long elevated waves. A trend can be observed in each graph except from (c), suggesting they should all be included in the runup analysis.

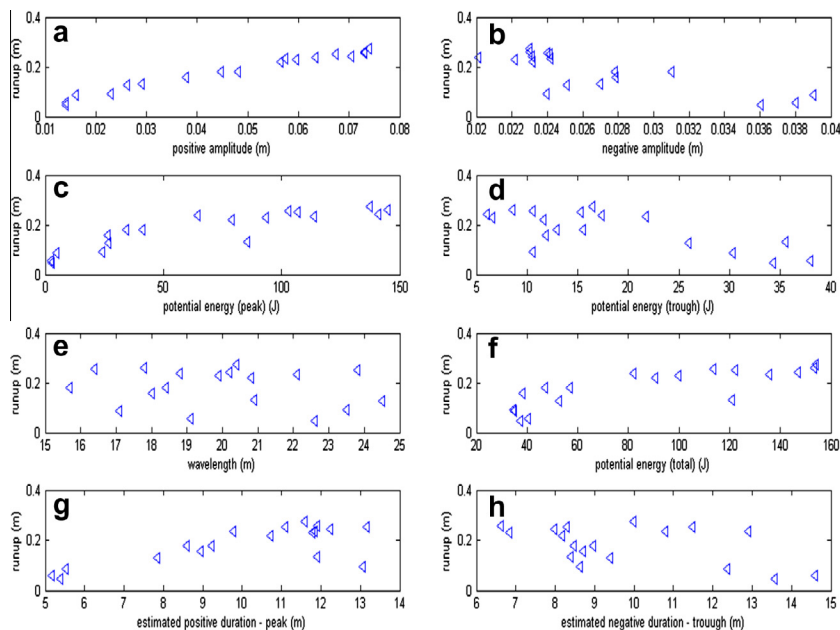


Fig. 8. Scatter plot of variables potentially influential on runup, here for long N-waves. A trend can be observed in all graphs except for wavelength. However for consistency with the analysis of elevated waves, all parameters are included in the N-wave runup analysis. The plot for positive and negative potential energy indicates that there is a balance between both potential energies during the wave runup process.

4.2. Correlations between runup and measures of the waveform

The next step is to look at the correlation between runup and measures characterizing the wave form for long and very long elevated, as well as N-waves. We aim to find a relationship between such measures and R . The present data is used for this purpose to test a large range of wavelengths.

4.2.1. Dimensional analysis

Figs. 7 and 8 confirm that for the data at hand, some correlation between runup and the parameters considered (potential energy, amplitude, wavelength) exists. One exception appears in Fig. 8(e) where there is no clear trend between wavelength and runup. A possible explanation is that the negative and positive wave components may not have an equal contribution to

the overall runup (as can be seen on Fig. 8(g) and (h)), with runup appearing more strongly dependent on positive duration of the wave and positively correlated, while the correlation is slightly weaker and negative for the duration of the trough wave, thus artificially masking the effect of the total wavelength. Therefore, for consistency with the analysis of elevated waves, the wavelength parameter will be included in the runup analysis of N-waves. A potential correlation between L , h and a was checked for in the case of the elevated waves generated in these experiments but without success. Therefore, L , h , a and a^- are independent variables for this dataset. Without any assumption on which of these parameters is the most influential on wave runup, a characteristic length parameter L^* can be introduced for the dimensional analysis. As three dependent potential energies can be considered (i.e., E_p , E_p^+ , E_p^-), a characteristic energy E^*

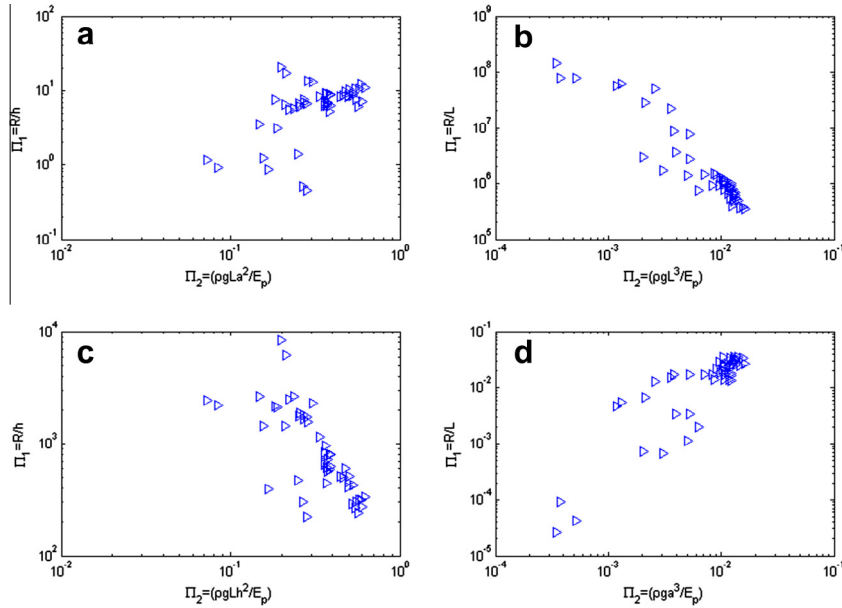


Fig. 9. Example correlations between the dimensionless products of equation (15) for different variables L^* . for all the data. These indicate a power law relates the two dimensionless products, where for (a) $L^* = L^{1/3}a^{2/3}$; (b) $L^* = L$; (c) $L^* = L^{1/3}h^{2/3}$; (d) $L^* = a$.

Table 4

Subpopulations of wave data for regression analysis, where l_b is the length of the beach, and T_b is the travel time of a linear wave along the length of the beach.

Notation	Description	Sample size (n)
$E \frac{T}{T_b} < 1$	Long elevated waves ($\frac{T}{T_b} < 1$)	21
$E \frac{T}{T_b} < 1$	Very long elevated waves ($\frac{T}{T_b} < 1$)	8
E	All elevated waves	29
$N \frac{T}{T_b} < 1$	Long N-waves ($\frac{T}{T_b} < 1$)	18
$N \frac{T}{T_b} < 1$	Very long N-waves ($\frac{T}{T_b} < 1$)	3
N	All N-waves	21

is also introduced. The functional relationship between the independent variables L^* , E^* , β , ρ , and g , can be expressed as:

$$R = f(L^*, E^*, \rho, g). \tag{13}$$

The beach slope parameter is a dimensionless quantity (and an invariant in the present experiments), therefore not included in (13). The Buckingham Pi theorem (Hughes, 1993) was applied to (13) and out of this analysis (see Charvet, 2012) two dimensionless groups, Π_1 and Π_2 , were formed:

$$\Pi_1 = \frac{R}{L^*}, \quad \Pi_2 = \frac{(L^*)^4 \rho g}{E^*}. \tag{14a, b}$$

Table 5

Elevated waves: wave group, response variable, combinations of k and $\log K$ giving a minimal value for equation (B2), coefficient of determination, mean of residuals and distribution of residuals for plots displaying a degree of linearity. The value in brackets next to the coefficient of determination indicates the number of outliers removed, if no value is shown, there were no outliers. The corresponding table for N-waves can be found in Charvet (2012).

$\frac{R}{L^*}$	L^{*3}	k	$\log K$	R^2	\bar{e}	$\{e_1, e_2, \dots, e_n\}$ Uncorrelated, $\sigma^2 = \text{constant}$	$\{e_1, e_2, \dots, e_n\}$ Normally distributed	
$E \frac{T}{T_b} < 1$	R/h	a^3	0.89	2.32	0.94(2)	-5.3×10^{-17}	Yes; yes	Yes
$E \frac{T}{T_b} < 1$	R/h	Lh^2	-0.45	1.97	0.87	6.7×10^{-16}	Yes; yes	No
$E \frac{T}{T_b} < 1$	R/h	h^3	-0.33	0.04	0.89	-6.3×10^{-17}	Yes; no	Yes
$E \frac{T}{T_b} < 1$	R/h	ah^2	-0.58	-0.49	0.87	-6.3×10^{-17}	Yes; yes	Yes
$E \frac{T}{T_b} < 1$	R/h	aLh	-0.56	1.71	0.96	-2.8×10^{-16}	Yes; yes	Yes
$E \frac{T}{T_b} < 1$	R/h	Lh^2	-0.33	1.33	0.96	-4×10^{-16}	Yes; yes	No
$E \frac{T}{T_b} < 1$	R/L	a^3	1.1	-0.88	0.91	-7×10^{-16}	Yes; yes	Yes
E	R/h	Lh^2	-0.37	1.47	0.84	4.9×10^{-16}	Yes; yes	Yes
E	R/L	aL^2	-0.59	0.15	0.92 (3)	2.7×10^{-16}	Yes; no	No
E	R/L	L^3	-0.44	1.53	0.95	6.7×10^{-16}	Yes; no	Yes

The characteristic length scale L^* may be the flume width (w), wave amplitude (a or a^-), height (H), wavelength (L), or water depth (h). As the present experiments were carried out in two dimensions, w can be taken as a unit width so the following equation applies here to a number of combinations of three possible variables for L^* . The functional relationship between the two groups can be expressed as:

$$\frac{R}{L^*} = \Psi \left(\frac{L^{*3} \rho g}{E^*} \right). \tag{15}$$

By plotting Π_1 against Π_2 for a sample of simple combinations of L^* , we can see that the data is best described by a power law (Fig. 9). All the data was used in these graphs. The cases where the correlation was poor were discarded. Therefore, we infer the functional relationship to be of the form:

$$\frac{R}{L^*} = K \left(\frac{L^{*3} \rho g}{E^*} \right)^k, \tag{16}$$

where K and k are coefficients empirically determined from the dataset. Regression analysis is necessary to identify the forms of (16) that can give a satisfactory fit to the data by optimizing values of K and k . Moreover, the scatter plots in Fig. 9 show that a signifi-

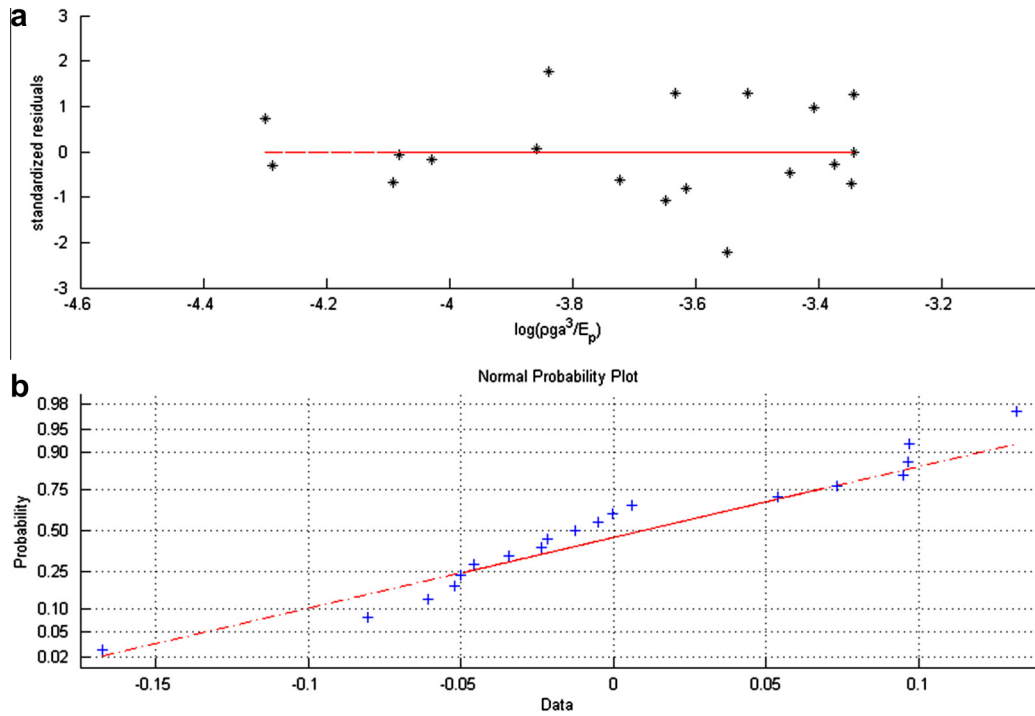


Fig. 10. (a) Residual plot corresponding to the best fit for wave group $E_{T_b}^T < 1$. This plot shows that the data is evenly distributed around the mean, within 2.5 standard deviations (i.e., good fit of the regression curve to the data). (b) Normal probability plot of the residuals: the normal distribution is represented by the red line, the corresponding distribution of the data is represented by the blue crosses. (For interpretation of the references to colour in this figure caption, the reader is referred to the web version of this article.)

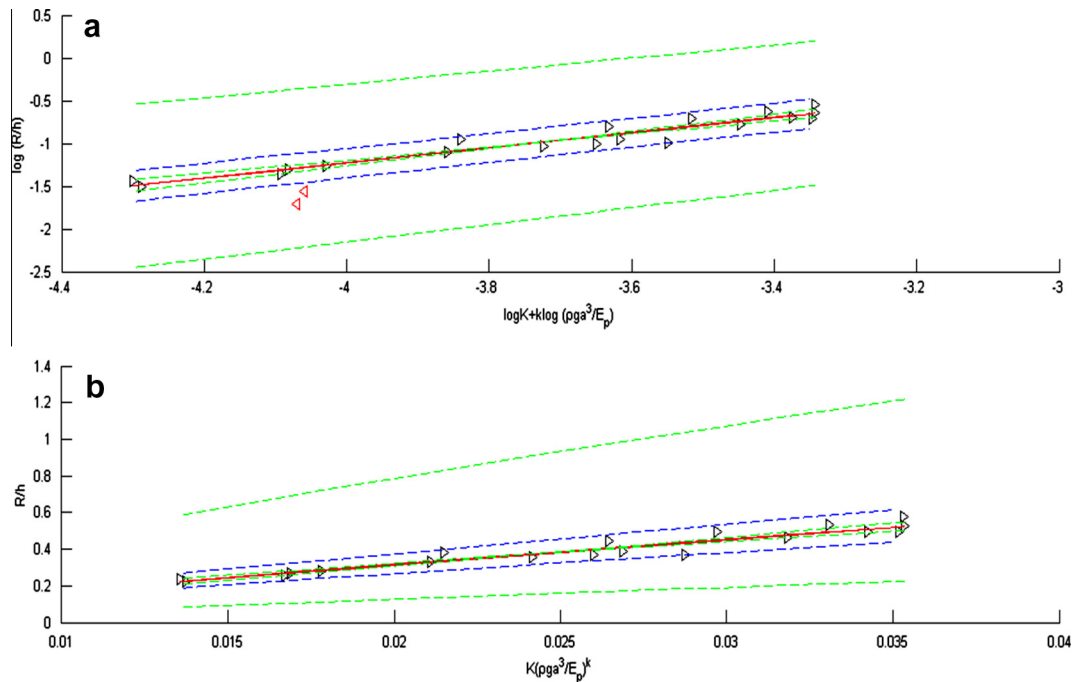


Fig. 11. Results of the regression analysis for wave group $E_{T_b}^T < 1$. (a) Equation (18) is represented in red, the 95% confidence intervals for the predicted variable are represented in blue dashes, and the 95% confidence intervals for the regression parameters are represented in green dashes (i.e., the maximum and minimum regression fit at this level of confidence is contained within the green asymptotes). The outliers (not taken into account in the regression) are represented in red. (b) Power law (19) and corresponding 95% confidence intervals for the predicted variable (in blue dashes), as well as 95% confidence intervals for the regression parameters k and K (in green dashes). The coordinates of the outliers (waves 6 and 7) are respectively (0.28; 0.21) and (0.27; 0.18). (For interpretation of the references to colour in this figure caption, the reader is referred to the web version of this article.)

Table 6

Power laws of the form of (23), with associated confidence intervals (C.I.), for the regression parameters k and K .

Wave group	Equation $\frac{R}{L} = K \left(\frac{\rho g L^3}{E_p} \right)^k$	C.I. k	C.I. K
$E_{T_b} < 1$	$\frac{R}{h} = 10.18 \left(\frac{\rho g a^3}{E_p} \right)^{0.89}$ (19)	(0.77; 1.00)	(6.51; 15.84)
$E_{T_b} > 1$	$\frac{R}{h} = 5.53 \left(\frac{E_p}{\rho g a L h} \right)^{0.5}$ (20)	(−0.68; −0.45)	(3.15; 9.80)
E	$\frac{R}{h} = 4.35 \left(\frac{\rho g a L h^2}{E_p} \right)^{-0.37}$ (21)	(−0.43; −0.31)	(2.84; 6.68)
$N_{T_b} < 1$	$\frac{R}{h} = 5.75 \left(\frac{E_p}{\rho g a L h^2} \right)^{0.4}$ (22)	(−0.44; −0.37)	(4.44; 7.39)
$N_{T_b} > 1$	$\frac{R}{a} = 0.27 \left(\frac{E_p}{\rho g a L h^2} \right)$ (23)	(−1.89; −0.44)	(0.19; 0.40)
N	$\frac{R}{a} = 10.7 \left(\frac{E_p}{\rho g a L (a^2)^2} \right)^{0.45}$ (24)	(−0.48; −0.43)	(9.78; 11.59)

cant proportion of the data tends to be clustered for large values of the predictor variable, which confirms the need for it to be partitioned into different wave categories.

4.2.2. Regression analysis

The uncertainty associated with (16) is quantified using a regression analysis. Linear regression can be performed using the variables in (16) by writing it as:

$$\log \left(\frac{R}{L^*} \right) = \log K + k \log \left(\frac{L^* \rho g}{E} \right) + \varepsilon. \quad (17)$$

It is necessary to find the best estimates (i.e., unbiased) for the regression coefficients of the model, thus minimize the uncertainty associated with the prediction. To do so, the total error between the response data and the predicted response is reduced (as described in Appendix B) and the non-violation of the relevant statistical assumptions is checked. More details on regression analysis methods can be found in Chatterjee and Hadi (2006). To capture potential differences in runup regime between long waves, very long waves, elevated waves and N-waves, the wave data is divided into different populations. Each wave group is identified with a letter, as listed in Table 4, and is used to find candidate runup equations, which are then compared. The following section details the procedure above for the first group of waves (Long elevated waves). The same procedure applies to every other group, therefore only the final runup equations are presented in this paper. Detailed information on the regression analysis for individual wave groups can be found in Charvet (2012).

The first subset of data to be used in the regression is long elevated waves (group $E_{T_b < 1}$). Only those combinations of k , K , L , h , and a that result in a high value of R^2 , a zero mean error, and which satisfy all the linearity assumptions, are kept. Table 5 presents the regression coefficients, characteristic lengths variables and uncertainties associated with the combinations displaying a significant degree of linearity between x and y ($R^2 \geq 0.80$).

In the present analysis, outliers are defined as data for which associated residuals are located more than 2.5 standard deviations away from their mean $\bar{\varepsilon}$ and they are removed. The methodology applied to verify the statistical assumptions presented in Table 5 is described in Appendix C.

The results of Table 5 indicate that for long elevated waves, there is a unique combination of the parameters a , h , L and E_p that gives a strong linear relationship ($R^2 = 0.94$) with unbiased estimates $\log K = 2.32$ and $k = 0.89$. These regression coefficients are close to 2 and 1 and are tested against the two null hypotheses: $H_{01} : \log K = 2$ and $H_{02} : k = 1$ (t -test). The t -test used for this purpose is described in Appendix D, and the results show that the runup relationship can be expressed as:

$$\log \left(\frac{R}{h} \right) = 2 + \log \left(\frac{a^3 \rho g}{E_p} \right). \quad (18)$$

This suggests that a linear relationship describes well the evolution of runup as a function of parameters of the wave form. The residual and normality plot associated with the regression are displayed in Fig. 10, and the 95% confidence intervals associated with the regression curve are also constructed (methodology described in Appendix E), and plotted together with the regression results in Fig. 11.

The same procedure is applied to all the other groups of waves. Laws of the form of Eq. (16) are summarized in Table 6, with confidence intervals for k and K , for each group of waves. The results from this table are discussed in the next section.

5. Discussion

The literature review has shown that a number of previous studies on runup of solitary/elevated waves have determined that the runup approximately scales as the amplitude of the incoming wave.

Posing $E_p \approx \rho g L a^2$, Eq. (19) indicates that: $\frac{R}{h} \propto \frac{a}{L}$. Moreover, $0.18 < K \frac{h}{L} < 0.53$ for all waves tested, suggesting that the runup of most of the present long elevated waves scales as the amplitude. Waves that are at the limit of the very long wave regime correspond to the smallest values of $\frac{h}{L}$; and we expect reflections from the beach to be significant, thus explaining why the amplitude scaling would appear weaker for some tests. The same reasoning can be applied to Eq. (22), showing that for long N-waves, $R \propto a$. However, given the confidence intervals for K the factor of proportionality would range from 4 to 7, indicating that for the same positive amplitude long N-waves would run up higher than long elevated waves (thus confirming the theoretical results from Tadepalli and Synolakis (1994)). A similar scaling $R \propto a$ can be obtained for all N-waves, which is expected, given that the very long N-waves group only contained 3 data points and therefore do not have a large influence.

For very long elevated waves (20), the best fit indicates a contribution of the wavelength that is of the same order as the amplitude. A simple explanation for this result would consist in considering the potential energy E_{p_s} of a mass of water m as it climbs up a beach with slope β which is:

$$E_{p_s} \approx \beta R m g. \quad (25)$$

In two dimensions, m can be approximated by $m \approx \rho a L$. Moreover, with β being constant and assuming $E_{p_s} \sim E_p$, we obtain:

$$\frac{R}{h} \sim \frac{E_p}{a L h \rho g}, \quad (26)$$

which is consistent with (20) in terms of the relative contributions of the different parameters at play.

Simplifying Eq. (20) we obtain $R \sim \sqrt{a}$. The present results suggest that there is a stronger dependence on wavelength for very long waves than for long waves, indicating the presence of two different regimes. The weaker dependence on amplitude for long waves may be due to the large amount of wave energy reflected back during the runup process.

As expected, the simplification of the runup equation for all elevated waves (21) does not point to any evident scaling of the runup with amplitude (or other wave parameter): the wave regimes having been shown to be different for the two groups.

Charvet (2012) did not find a strong correlation between runup and rundown, for long N-waves. For very long N-waves, not enough data was collected to give conclusive results. However, drawing lines of best fit through the long and very long N-wave data, respectively, would indicate a decrease in runup with an increase in rundown. This would be consistent with the trends in Fig. 8(d)). It has to be noted that the range of troughs that could

be generated, especially for long waves, was small, so such results should be interpreted with caution.

The aim of investigating a possible common relationship for all wave forms would require more test data concerning very long elevated and N-wave data (smaller samples for these groups at present). Notwithstanding, a common relationship for all wave forms may not exist in reality. Indeed, the results indicate that the runup of elevated waves and the runup of N-waves should be treated as two separate processes, as the negative components of N-waves (a^- , E_p^-) often appear in the best fit.

6. Conclusions

The impact of long propagating waves is often assessed using runup. For this reason, researchers have strived to obtain empirical or semi-empirical formulae that help predict the runup of long waves. Validation of runup laws with laboratory data or numerical codes is common. The runup of long propagating waves has been derived empirically mainly as a function of wave amplitude, water depth, and bed slope, whether we consider a propagating bore, a solitary/elevated or N-wave shape.

The data obtained with the new pneumatic generator was used to find new runup relationships including parameters that have not been studied experimentally before. A semi-empirical approach was chosen to investigate the relationship between wave runup and a number of parameters characterizing the wave form (i.e., positive and negative amplitudes, wave height, wavelength, water depth, potential energy). Dimensional analysis was first used to relate these parameters to runup. The relationship identified was a power law. Next, simple linear regression analysis was used to find the combination of parameters resulting in the best fit to the experimental data. Expressions for runup were derived separately for long elevated waves, long N-waves, very long elevated waves, and very long N-waves. The resulting expressions are seen to be consistent with previous studies, for long waves (elevated and N-waves), with the runup seen to be scaled as the positive amplitude ($R \sim a$). However, very long waves are shown to belong to a different regime than long waves, and to scale as $R \sim \sqrt{a}$. This result has been suggested also by Baldock and Holmes (1999) for bore-like waves. It is believed that potential energy is a useful addition to the parameters predicting runup.

More systematic studies of the influence of slope variations on long wave runup dynamics are needed to clarify the relative contribution of the beach slope in comparison with wave parameters.

Acknowledgements

This work was funded by the UK Engineering and Physical Sciences Research Council. We also gratefully acknowledge Professor William Allsop and the staff at HR Wallingford for providing the authors with access to the facility, support during the testing of the pneumatic generator, and contribution in terms of manpower and experimental equipment. Finally, the authors wish to thank the reviewers of this manuscript, particularly Dr Yong Sung Park, whose time in providing insightful comments and suggestions was greatly beneficial to the present work.

Appendix A

The repeatability of waves was tested by running the same tests a number of times (for both elevated and N-waves). Each sample is composed of 3 to 6 repeats of one given wave, and the variance in a chosen wave parameter x (s_x^2) is:

$$s_x^2 = \frac{\sum (x_i - \bar{x})^2}{N - 1}, \quad (\text{A1})$$

To obtain the standard deviation in x for a range of waves, it is necessary to combine all samples. To do so, we calculate the pooled variance and standard deviation s_{p_x} for the combined samples (Moore and Mc Cabe, 2003), after verifying the largest standard deviation is not larger than twice the smallest standard deviation for each sample in the pool.

$$s_{p_x} = \sqrt{\frac{\sum_{i=1}^n (n_i - 1) s_{i_x}^2}{\sum_{i=1}^n (n_i - 1)}}. \quad (\text{A2})$$

Taking x as a for positive amplitude, a^- for negative amplitude, T for period and R for runup, the standard deviations of these different variables are listed in Table 3. There were nine individual elevated waves and 4 N-waves to calculate the pooled standard deviations for amplitudes and period. There were 26 runup standard deviations calculated for elevated waves and 18 for N-waves. These results make no assumption on the variations of wave amplitudes further down the flume (i.e., it is expected that σ_a will increase with x).

Appendix B

To find the best estimates of $\log K$ and k the residuals, e_i , have to be calculated and the sum of squared residuals, SSE , has to be minimized:

$$e_i = y_i - \hat{y}_i, \quad (\text{B1})$$

$$SSE = \sum_{i=1}^n e_i^2. \quad (\text{B2})$$

In (B1) and (B2), for n data points, y_i is one observed response to an input variable x_i , and \hat{y}_i is the response predicted by (17) (for $\varepsilon \approx 0$).

We define the uncertainty associated with (17) as being minimal when the coefficient of determination, R^2 , approaches 1 and the mean of the deviations (squares) from the fit \bar{e} is zero. R^2 indicates the proportion of the total variability in the response variable which is accounted for by the predictor variable (Chatterjee and Hadi, 2006). The coefficient of determination is calculated using the total sum of squares, SST :

$$SST = \sum_{i=1}^n (y_i - \bar{y})^2, \quad (\text{B3})$$

$$R^2 = 1 - (SSE/SST), \quad (\text{B4})$$

The mean error is expressed as:

$$\bar{e} = \frac{\sum_{i=1}^n e_i}{n}. \quad (\text{B5})$$

Appendix C

The normal distribution of residuals has been checked in two ways. First, a normal probability plot was used to graphically assess the fit of the data to a normal distribution (Fig. 10 -b)). If the data only deviated slightly from the normal distribution, an additional conservative statistical test of normality, Lilliefors (1967), was performed to test the null hypothesis H_0 : the residuals are normally distributed:

$$D = \max_e |F^*(e) - S_n(e)|. \quad (\text{C1})$$

In (C1), $F^*(e)$ is the cumulative normal distribution function with mean \bar{e} and standard deviation s_e^2 , and $S_n(e)$ is the sample's cumulative distribution function. To validate H_0 , D shall not exceed a critical value, the latter is determined according to the sample size n and the level of significance desired α . α represents the probability that the test will reject H_0 when it is in fact true (Moore and Mc

Cabe, 2003). In the examination of residuals, we choose to detect not only pure normal distributions but close to normal distributions so we set $\alpha = 0.001$. If the residuals follow a normal distribution, the equation is rated as “Yes” in the last column of Table 5.

In addition, standardized residuals have been plotted against the predictor variable to detect any violation of the linearity assumption: if the assumption holds, no correlation should be detected. The standardized residuals z_i are easier to interpret than the ordinary residuals e_i , as they are centered and scaled as follows:

$$z_i = \frac{e_i - \bar{e}}{\sigma} \tag{C2}$$

In (C2), the standard deviation of the residuals σ can be calculated from the estimated variance of the residuals, and given by:

$$\sigma^2 = SSE/(n - 2). \tag{C3}$$

The plot of the residuals against x allows to visually check that there is no heterogeneity of σ^2 (Fig. 10 -a)).

Appendix D

The regression coefficients of the fit for long elevated waves are close to 2 and 1, they are tested against the two null hypotheses: $H_{0_1} : \log K = 2$ and $H_{0_2} : k = 1$. The testing of hypotheses is done using a t -test as (see Chatterjee and Hadi, 2006). A t -test can be applied providing $n \gg 15$; if $n \approx 15$ and outliers have been removed, or if $n < 15$ and the response variable is normally distributed (Moore and Mc Cabe, 2003). In other cases, this test should not be used. For wave group $E_{T < 10}$, (two outliers for Eq. (25), $n = 19$). The test statistic requires the calculation of the standard errors associated with k and $\log K$:

$$SE_{\log K} = \sqrt{\sigma^2 \left(\frac{1}{n} + \frac{x^2}{\sum_{i=1}^n (x_i - \bar{x})^2} \right)}, \tag{D1}$$

$$SE_k = \sqrt{\frac{\sigma^2}{\sum_{i=1}^n (x_i - \bar{x})^2}}, \tag{D2}$$

$$t_{\log K} = \frac{\log K - C_{\log K}}{SE_{\log K}}, \tag{D3}$$

$$t_k = \frac{k - C_k}{SE_k}. \tag{D4}$$

In (D1) and (D2), an unbiased estimate of the variance of the residuals is given by (C3), and the t statistics (D3) and (D4) are distributed as a Student’s t with $n - 2$ degrees of freedom (Chatterjee and Hadi, 2006). $C_{\log K}$ and C_k are the constants chosen, to be compared with $\log K$ and k , respectively. If the magnitude of the t statistic is greater than the critical value from the t distribution $t_{(n-2, \alpha/2)}$, then the corresponding null hypothesis (in our case, H_{0_1} or H_{0_2}) is rejected. The t values distribution table (used for all wave groups) can be found in SEMATECH, 2006. For all wave groups we choose a level of significance $\alpha = 0.01$, so for long elevated waves $t_{(95, 0.005)} = 2.898$. We obtain $|t_{\log K}| = 1.51$ and $|t_k| = 2.00$. Hence, both hypotheses are validated.

Appendix E

When the errors are normally distributed, it is possible to construct the confidence intervals for the regression parameters ($\log K$ and k) of Eq. (17). Confidence intervals are expected to contain the true value of the parameter of interest at the level of confidence chosen. The $(1 - \alpha) \cdot 100\%$ confidence interval for $\log K$ and k , respectively are given by Chatterjee and Hadi (2006):

$$\log K \pm t_{(n-2, \alpha'/2)} SE_{\log K}, \tag{E1}$$

$$k \pm t_{(n-2, \alpha''/2)} SE_k. \tag{E2}$$

We choose here to obtain 95% confidence intervals for $\log K$ and k using (E1) and (E2). The $(1 - \alpha'') \cdot 100\%$ confidence interval for the prediction of response variables \hat{y}_{0_i} for a range of chosen variables x_{0_i} , is:

$$\hat{y}_{0_i} \pm t_{(n-2, \alpha''/2)} SE_{\hat{y}_{0_i}}, \tag{E3}$$

With

$$SE_{\hat{y}_{0_i}} = \sqrt{\sigma^2 \left(1 + \frac{1}{n} + \frac{(x_{0_i} - \bar{x})^2}{\sum_{i=1}^n (x_i - \bar{x})^2} \right)}. \tag{E4}$$

Because the regression results are only valid between the minimum and maximum values of x tested, confidence intervals for the whole range of values $x_{\min} < x_{0_i} < x_{\max}$ are constructed and plotted in Fig. 11 along with the regression fit (18) and the confidence intervals for the regression parameters. Here we choose $\alpha' = \alpha''$ so 95% confidence intervals for the regression parameters and the prediction variable are obtained.

Appendix F

Test	a	a^-	h	T/Tb	Tb
1	0.083	0.000	0.45	0.75	13.04
2	0.076	0.000	0.45	0.53	13.04
3	0.065	0.000	0.45	0.49	13.04
4	0.045	0.000	0.45	0.35	13.04
5	0.054	0.000	0.45	0.48	13.04
6	0.030	0.000	0.45	0.44	13.04
7	0.027	0.000	0.45	0.42	13.04
8	0.076	0.000	0.52	0.67	12.17
9	0.070	0.000	0.52	0.66	12.17
10	0.067	0.000	0.52	0.58	12.17
11	0.054	0.000	0.52	0.76	12.17
12	0.053	0.000	0.52	0.52	12.17
13	0.032	0.000	0.52	0.41	12.17
14	0.024	0.000	0.52	0.35	12.17
15	0.080	0.000	0.57	0.78	11.58
16	0.072	0.000	0.57	0.73	11.58
17	0.070	0.000	0.57	0.72	11.58
18	0.048	0.000	0.57	0.70	11.58
19	0.035	0.000	0.57	0.45	11.58
20	0.033	0.000	0.57	0.43	11.58
21	0.027	0.000	0.57	0.41	11.58
22	0.042	0.000	0.45	1.31	13.04
23	0.039	0.000	0.52	1.10	12.17
24	0.027	0.000	0.52	1.09	12.17
25	0.072	0.000	0.57	1.00	11.58
26	0.028	0.000	0.57	1.59	11.58
27	0.100	0.000	0.56	4.46	11.74
28	0.110	0.000	0.56	6.54	11.74
29	0.110	0.000	0.56	7.85	11.74
30	0.074	0.023	0.46	0.68	12.90
31	0.073	0.023	0.46	0.54	12.90
32	0.073	0.024	0.46	0.57	12.90
33	0.048	0.031	0.50	0.56	12.37
34	0.029	0.027	0.53	0.69	12.02
35	0.016	0.039	0.55	0.63	11.80

(continued on next page)

(continued)

Test	a	a^*	h	T/T_b	T_b
36	0.057	0.024	0.61	0.77	11.20
37	0.059	0.022	0.61	0.62	11.20
38	0.056	0.023	0.61	0.63	11.20
39	0.038	0.028	0.62	0.62	11.11
40	0.023	0.024	0.63	0.75	11.02
41	0.014	0.036	0.64	0.71	10.94
42	0.067	0.024	0.65	0.81	10.85
43	0.070	0.023	0.65	0.64	10.85
44	0.063	0.020	0.65	0.79	10.85
45	0.045	0.028	0.66	0.64	10.77
46	0.026	0.025	0.68	0.62	10.61
47	0.014	0.038	0.69	0.73	10.53
48	0.028	0.338	0.61	9.52	11.25
49	0.022	0.257	0.53	8.27	12.04
50	0.024	0.255	0.53	14.26	12.04

References

- Baldock, T.E., Holmes, P., 1999. Simulation and prediction of swash oscillations on a steep beach. *Coastal Engineering* 36, 219–242.
- Borthwick, A.G.L., Ford, M., Weston, B.P., Taylor, P.H., Stansby, P.K., 2006. Solitary wave transformation, breaking and runup at a beach. *Maritime Engineering* 159 (MA3), 97–105.
- Carrier, G.F., Greenspan, H.P., 1958. Water waves of finite amplitude on a sloping beach. *Journal of Fluid Mechanics* 17, 97–110.
- Charvet, I., 2012. Experimental modelling of long elevated and depressed waves using a new pneumatic wave generator. PhD thesis, University College London.
- Chatterjee, S., Hadi, A.S., 2006. *Regression Analysis by Example*, 4th ed. Wiley & Sons, Hoboken, New Jersey, USA.
- Fuhrman, D.R., Madsen, P.A., 2008. Surf similarity and Solitary wave runup. *Journal of Waterway, Port, Coastal and Ocean Engineering* 134 (3), 195–198.
- Grilli, S.T., Subramanya, R., Svendsen, I.A., Veeramony, J., 1994. Shoaling of solitary waves on plane beaches. *Journal of Waterway, Port, Coastal and Ocean Engineering* 120 (6), 609–628.
- Hall, J.V., Watts, G.W., 1953. Laboratory investigation of the vertical rise of solitary waves on impermeable slopes. Army Coastal Engineering Research Center, Washington DC, Tech. Memo 33.
- Kaplan, K., 1955. Generalized laboratory study of tsunami run-up, US army corps of engineers, Tech Memo, 60.
- Klettner, C., 2010. On the fundamentals principles of waves propagating over complex geometry. PhD Thesis, University College London.
- Klettner, C., Balasubramanian, S., Hunt, J.C.R., Fernando, H.J.S., Voropayev, S., Eames, I., 2012. Drawdown and run-up of tsunami waves on sloping beaches. *Engineering and Computational Mechanics* 165 (EM2), 119–129.
- Klettner, C., Eames, I., 2012. The laminar free surface boundary layer of a solitary wave. *Journal of Fluid Mechanics* 696 (423), 433.
- Kobayashi, N., Cox, D., Wurjanto, A., 1990. Irregular wave reflection and run-up on rough impermeable slopes. *Journal of Waterway, Port, Coastal and Ocean Engineering* 116 (6), 708–726.
- Kobayashi, N., Lawrence, R., 2004. Cross shore sediment transport under breaking solitary waves. *Journal of Geophysical Research* 109 (No. C03047).
- Li, Y., Raichlen, F., 2002. Non-breaking and breaking solitary wave run-up. *Journal of Fluid Mechanics* 456, 295–318.
- Li, Y., Raichlen, F., 2003. Energy Balance model for breaking solitary wave runup. *Journal of Waterway, Port, Coastal and Ocean Engineering* 129 (2).
- Lilliefors, H.W., 1967. On the Kolmogorov–Smirnov test for normality with mean and variance unknown. *Journal of the American Statistical Association* 62 (138), 399–402.
- Longuet-Higgins, M.S., 1974. On the mass, momentum, energy and circulation of a solitary wave. *Proceedings of the Royal Society of London Series A, Mathematical and Physical Sciences* 337, 1–13.
- Madsen, P.A., Fuhrman, D.R., Schaffer, H.A., 2008. On the solitary wave paradigm for tsunamis. *Journal of Geophysical Research* 113, 1–22, C12012.
- Madsen, P.A., Schaffer, H.A., 2010. Analytical solutions for tsunami runup on a plane beach: single waves, N-waves and transient waves. *Journal of Fluid Mechanics* 645, 27–57.
- Moore, D.S., McCabe, G.P., 2003. *Introduction to the Practice of Statistics*, 4th edn. Freeman, New York.
- Nassirpour, S., 2012. Analysing Post Tsunami Data. MSc Thesis, University College London.
- NIST/SEMATECH, 2006. *Engineering Statistics Handbook*. <<http://www.itl.nist.gov/div898/handbook/>> (Date accessed: 01–10–2011)
- Plafker, G., 1965. Tectonic deformation associated with the 1964 Alaskan earthquake. *Science* 148 (3678), 1675–1687.
- Rossetto, T., Allsop, W., Charvet, I., Robinson, D., 2011. Physical modelling of tsunamis using a new pneumatic wave generator. *Coastal Engineering* 58, 517–527.
- Shen, M.C., Meyer, R.E., 1963. Climb of a bore on a beach. Part 3 Run-up. *Journal of Fluid Mechanics* 16, 113–125.
- Shuto, N., 1967. Run-up of long waves on a sloping beach. *Coastal Engineering in Japan* 10, 23–38.
- Synolakis, C.E., 1986. *The Runup of Long Waves*. PhD thesis, California Institute of Technology.
- Synolakis, C.E., 1987. The runup of solitary waves. *Journal of Fluid Mechanics* 185, 523–545.
- Tadepalli, S., Synolakis, C.E., 1994. The run-up of N-waves on sloping beaches. *Mathematical and Physical Sciences* 445 (1923), 99–112.
- Tadepalli, S., Synolakis, C.E., 1996. Model for the leading waves of Tsunamis, *Physical Review Letters*, vol. 77, no. 10.
- Togashi, H., 1981. Study on tsunami run-up and countermeasure. PhD thesis, Tohoku University.
- Zelt, J.A., 1991. The run-up of nonbreaking and breaking solitary waves. *Coastal Engineering* 15 (205), 246.